# Efficient Implementation of the Spectral Domain Method Including Precalculated Corner Basis Functions

S. A. Meade and Chris J. Railton, *Member, IEEE*

***Abstract*— A general implementation of the Spectral Domain Method, formulated for planar microstrip circuits of arbitrary metallisation pattern is presented. The inclusion of *a priori* knowledge of the edge and corner singularities in the set of basis functions results in a large decrease in the order of the problem to be solved. Libraries of basis functions allow the rapid rigorous analysis of realistically complex circuits. Calculated $S$-parameters are given for three microstrip lowpass filters and compared to results from both measured data and other techniques.**

## I. Introduction

The rigorous full-wave analysis of complex planar microwave components and circuits has been made possible due to large increases in computing power and the development of a number of numerical and semi-analytic techniques. However, the complexity of circuits to be analysed is increasing rapidly, along with a need for an interactive design technique rather than an analysis tool. Therefore a method is required which combines the rigorous nature of full-wave analysis with the rapid solution available from quasi-static models.

The spectral domain method (SDM) has been widely implemented for the rigorous analysis of microwave passive planar circuits. It has been shown [1] that the use of rooftop current basis functions allows an irregular metallisation pattern to be defined. As with other techniques [2], [3] the widespread application of the method is limited by the requirement for a large amount of computer resources.

In [4], it was proposed an efficient algorithm based on the SDM (with rooftop basis functions) which exploited the asymptotic behavior both of the Green's function and of the current distribution, thus dramatically reducing the CPU time required for a given problem. Precomputed basis functions were limited to isolated microstrip resonators. In this contribution the basic algorithm has been extended to allow the treatment of more complex structures, modelled using precomputed current basis functions.

It is envisaged that a library of such functions will allow the rapid rigorous analysis of complex metallisation patterns, with improvements in run-times of the order of 100 to 1000 over that of the original rooftop basis function algorithm [1]. With the number of basis functions reduced, approximately from 1000 to 100, the need to implement an iterative solution to the resulting matrix equation (e.g. conjugate gradient method [5]) has been eliminated at the present level of circuit complexity. Moreover, to the authors' knowledge this is the first time that corner singularities have been included, using precalculated basis functions, in such a general implementation of SDM.

In the following sections, the formulation of the technique is outlined, with emphasis on the features which improve efficiency and run-times. The definition of precalculated basis functions as a linear combination of the rooftop functions and the inclusion of *a priori* knowledge of current distribution is explained in Section III. In Section IV a method to extract a frequency independent function to define corner singularities is introduced for the first time to authors' knowledge. Examples are given of the application of the method for two microstrip filters. Comparison is made to the original rooftop basis function model which does not include precomputed basis functions, other published results and measured data.

Manuscript received March 23, 1993; revised October 25, 1993. The authors are with the Centre for Communications Research, Faculty of Engineering, University of Bristol, Bristol, BS8 1TR, U.K.
IEEE Log Number 9404106.

## II. Equations

As in [4] a Method of Moments solution, formulated in the spectral domain, applied to a planar structure leads to the following set of equations:

$$\sum_s a_s Z_{\mathrm{st}} = V_t \qquad \text{for all } t \tag{1}$$

where the elements of the impedance matrix are

$$Z_{\mathrm{st}} = \sum_{n,m}^{N,M} \left( \tilde{w}_t(n,m)(\tilde{G}(n,m,w) - \tilde{G}^{\infty}(n,m))\tilde{J}_s(n,m) \right) + Z_{\mathrm{st}}^{\infty} \tag{2}$$

and

$J_s(x,y)$ is the set of current basis functions
$w_t(x,y)$ is the set of weighting functions
$G(w)$ is the dyadic Green's function
indicates the Fourier transform
$\tilde{V}_t$ is the excitation vector

and the asymptotic part of the impedance matrix

$$Z_{\mathrm{st}}^{\infty} = h_{\mathrm{st1}} Z_{\mathrm{st1}}^{\infty} + h_{\mathrm{st2}} Z_{\mathrm{st2}}^{\infty} \tag{3}$$

and

$$\tilde{G}^{\infty}(n,m) = h_{\mathrm{st1}} K_{\mathrm{st1}}^{\infty}(n,m) + h_{\mathrm{st2}} K_{\mathrm{st2}}^{\infty}(n,m) \tag{4}$$

is the asymptotic form of the Green's function for large $n$ and $m$ [4], [6]. See Appendix A for further definition of terms.

A Fast Fourier Transform algorithm is used to efficiently calculate the asymptotic part of the impedance matrix ($Z_{\rm st}^{\infty}$ in (2)) as described in [4]. $Z_{\rm st1}^{\infty}$ and $Z_{\rm st2}^{\infty}$ (see Appendix A and [4]) in (3) are actually calculated by the FFT routine and saved to file; both are independent of frequency. Then $h_{\rm st1}$ and $h_{\rm st2}$ are calculated once per frequency and are independent of the geometry. The summation in equation converges rapidly and $N$ (and $M$) of the order of 20 is sufficient in many cases.

Symmetries in the impedance matrix ($Z_{\rm st}$ in (1)) are included in the algorithm similar to [1]

$$Z_{xx}(i,j) = Z_{xx}(j,i) \quad \text{similarly for } Z_{yy}$$
$$Z_{yx} = -Z_{xy}.$$

The same symmetries are used in the asymptotic impedance matrix FFT algorithm. Moreover, an additional symmetry is now possible to further reduce the computational effort. That is, only $Z_{xy}^{\infty}(i,j)$ $(i \geq j)$ is directly calculated, details are given in Appendix B.

## III. Current Basis Functions

The FFT algorithm [4] used to efficiently calculate the asymptotic sums in (2) assumes that the sub-domain basis functions are identical apart from a shift in origin. The rooftop functions preferred in this implementation differ from those commonly used [1], [7], [8] in the direction perpendicular to the current flow. Fig. 1(a) illustrates a rooftop function to model current flow in the $y$-direction, the step function in this research is $2 * l_x$ wide ($l_x$ is the grid size in $x$ direction) compared to $l_x$ in [1], [7], [8]. Thus the functions overlap in both directions in contrast to the previous case of only in the direction of current flow. Fig. 1(b) and (c) show three rooftop functions and illustrate a typical transverse current distribution for a microstrip line. The centrally located rooftop 3 overlaps both adjacent functions (rooftops 1 and 2) and is opposite in magnitude, the resultant current distribution in Fig. 1(c) is equivalent to a set of four nonoverlapping rooftops. This arrangement allows the co-location of the $x$ and $y$ grids, with no loss in generality of the functions. Comparisons with a version of the technique using nonoverlapping step functions and corresponding offset $x$ and $y$ grids clearly illustrates the equivalence of the two techniques (see Section V).

The proposed rooftops have the advantage of a minimum distance between rooftops of $l_x$ whereas the latter $l_x/2$ is needed due to the offset grids, thus the number of difference terms [4, Appendix] is reduced by half, with a corresponding improvement in efficiency of the FFT algorithm.

The rooftop functions can be combined to form a single function. The FFT algorithm to rapidly calculate $Z_{\rm st}^{\infty}$ is still valid for a combined basis function. Moreover, *a priori* knowledge of the current distribution can be included in such a function. Reference [4] introduced the concept of precomputed basis functions for the modes of microstrip resonators. This is now expanded to allow a set of arbitrary basis functions to be defined

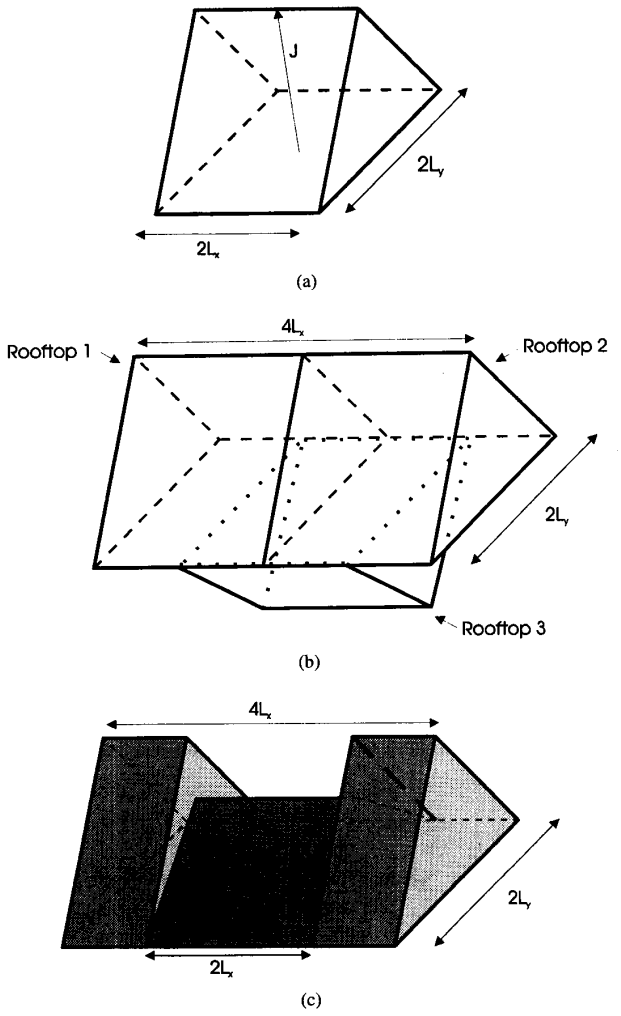


Fig. 1. Overlapping step rooftop current basis function.

$$J(r) = \sum_{p=1}^{P} b_p \psi_p(r) \tag{5}$$

where $\psi_p(r)$ the current distribution of the $p^{\rm th}$ basis function is

$$\psi_p(r) = \sum_{q=1}^{Q} a_{pq} R_q(r). \tag{6}$$

Thus, an algorithm has been defined which allows current basis functions ($\psi_p$) to be expressed as a linear combination of rooftop functions ($R_q$). It is now proposed that such a set of basis functions can be derived which fully describe the response of relatively complex metallisation patterns.

The current standing wave set up on a straight microstrip line is modelled as a set of line modes.

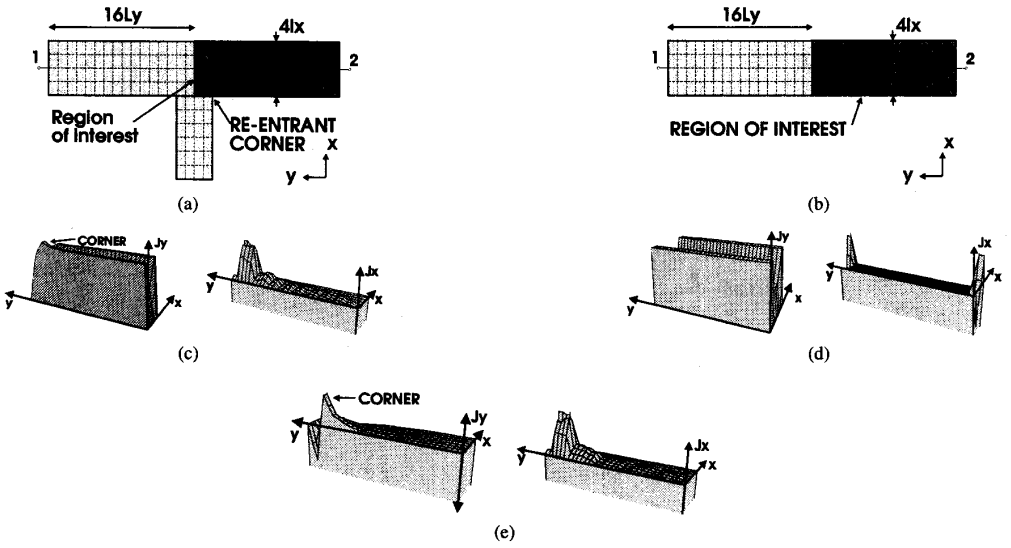


Fig. 2. Example of derivation of corner basis function.

The variation of the current distribution in the direction of current flow is given by

$$\begin{aligned} J_y^d(x,y) &= \cos(d\pi y/L)J_y^p(x) \quad \text{odd line modes} \\ &\quad \sin(d\pi y/L)J_y^p(x) \quad \text{even line modes} \\ J_x^d(x,y) &= \sin(d\pi y/L)J_x^p(x) \quad \text{odd line modes} \\ &\quad \cos(d\pi y/L)J_x^p(x) \quad \text{even line modes} \end{aligned} \tag{7}$$

for the $d^{\text{th}}$ line mode. Where $d = 0$ to $D$ for odd line modes, $d = 1$ to $D$ for even line modes, $L$ is the length of the microstrip line and $J_s^p(x)$ ($s = x$ or $y$) is the current distribution along the line perpendicular to current flow, precalculated by a two dimensional version of the technique [4].

Each line mode can be represented by a precalculated basis function with $x$ and $y$ components. The number of modes required to fully describe a given length of line is restricted by the minimum microstrip guide wavelength ($\min.\lambda_g$) to be modelled. That is the minimum line mode wavelength ($\lambda_D$) is less than the minimum microstrip guide wavelength required

$$\lambda_D < \min.\lambda_g \tag{8}$$

where $\lambda_D$ is the wavelength of the highest order line mode and the wavelength of the $d^{\text{th}}$ line mode is given by

$$\lambda_d = 2 * L/d. \tag{9}$$

The microstrip guide wavelength ($\lambda_g$ in (8)) is taken as the wavelength for an infinite line and calculated by a two dimensional version of the technique. A simple database has been set up which holds the wavelength for different substrates and line widths etc. This allows the user to just define the maximum frequency of interest, the number of modes required for all lines is then automatically calculated.

## IV. Corner Basis Functions

The analysis of arbitrary circuits involves dividing the metallisation into regions. In each region we define a set of basis functions which we will call region basis functions. For the microstrip stub in Fig. 2(a) the highlighted region 1 is modelled by a set of basis functions which include the line modes defined by (7).

However, the set of line modes defined above are not sufficient to model metallisation discontinuities. It is possible to add extra rooftop functions in the area of a discontinuity but this approach results in relatively high numbers of basis functions; also the effect of a discontinuity can be significant along a large portion of a circuit, reducing the technique to that of a basic rooftop algorithm.

The inclusion of *a priori* knowledge of the perturbation of the current distribution in the set of region basis functions, reduces the order of the problem. The number of basis functions ($P$ in (5)) is reduced from the order of 1000's to 100's (or less) for realistically complex circuits. Thus the order of the matrix equation (1) to be solved has been decreased.

A technique has been developed to "extract" the required function from a low frequency solution of the current distribution for a single corner by comparison to a similar structure which does not contain the discontinuity. Only a single function ($x$ and $y$ components) is required to model the corner over the full frequency range of interest. A database of such functions is used to then model a wide range of metallisation patterns as the function depends only on the geometry of the corner.

Considering the highlighted region as an example, Fig. 2 illustrates the process for an arbitrary reentrant corner. Two metallisation patterns are shown in Fig. 2(a) and (b), the former is a simple microstrip stub whereas the latter is a microstrip line with the same dimensions as the feedlines of the stub. Rooftops (Fig. 1) are required as the basis functions for the

microstrip stub (a) but line modes ((7) are assumed for the microstrip line (b). The excitation vector ($V_t$ in (1)) is set to give a source at port 1. Then for both metallisation patterns, (1) is solved for the set of coefficients ($a_s$ in (1)) at one spot frequency (less than the frequency band of interest). The resultant current distributions on the region of interest are plotted in Fig. 2(c) and (d). The current distribution for the microstrip line clearly shows the edge singularity included in the line mode basis functions, the current component in the $x$ direction is an order of magnitude less but is included for completeness of solution. The edge singularity is evident in the corresponding region of feedline of the microstrip stub, except in the portion next to the stub. Moreover, the reentrant corner singularity can be clearly distinguished. A simple subtraction of the two normalised current distributions results in the distribution shown in Fig. 2(e). This is the required function which includes the corner singularity. Moreover, the function compensates for the lack of edge discontinuity assumed by the line modes.

Thus a function has been derived which fully describes the perturbation of the current due to a corner over the full frequency band of interest. Moreover the function depends only on the geometry of the corner itself, not on the surrounding circuitry. That is, only the relative dimensions in a region are required to be the same (in the above example $4l_x$ by $16l_y$). The function is also independent of substrate permittivity and thus reduces the necessity to define new functions for new circuits.

The above approach results in a set of functions which fully describe a region, each function only differs from another in a set by the individual weights ($a_{pq}$ in (6)) of the constituent rooftop functions. Therefore both routines to calculate the Fourier transform of the current and the asymptotic impedance matrix ($\tilde{J}(n,m)$ and $Z_{\text{st}}^{\infty}$ in (2)) use this fact to form efficient implementations.

The set of basis functions for the other regions of the circuit in Fig. 2(a) are derived with a similar procedure. Moreover, an identical set of basis functions can be used for the input region as previously derived for the output region except the precomputed corner function in Fig. 2(e) is mirrored in the $y = 0$ line. The stub region is modelled by a set of resonant modes as basis functions (similar to [4]) and a precomputed basis function for each corner. The transition of the current between each region is achieved using either rooftop functions or another set of precomputed basis functions. Thus in the stub example an inverted "$T$" shaped area is defined by rooftop functions which overlap one sub-domain into each region.

## V. Simple Lowpass Filter

Results are available in literature for the microstrip lowpass filter [2] shown in Fig. 3. This filter is analysed to demonstrate the equivalence of the overlapping step rooftops used here, the nonoverlapping step rooftop [1, 7, 8] and the proposed region basis functions. The efficiency of the latter approach is highlighted.

For this purpose only a coarse grid is utilised in the first model ($l_x = l_y = w_1/4 = w_2/4 = 0.635$ mm, $l_1 = 5.715$ mm and $l_2 = 3.81$ mm in Fig. 3). Comparison to published results is limited by this approximation and by the assumed fully shielded structure in this implementation [4] in contrast to the the open structure in [2]. Results for the magnitude of the $S$-parameters for overlapping and nonoverlapping step basic rooftop models are plotted in Fig. 5. It is evident that the two versions are equivalent, with the slight shift in response curves due to the different convergence patterns of the techniques. The overlapping step requires only 135 rooftop functions ($x$ and $y$ components); whereas the nonoverlapping step needs 160 rooftops for the same definition. Moreover, the overlapping step rooftops require fewer difference terms (10). Both implementations do not fully agree with the measured [2] response curve this is due to the coarse grid and the closed nature of the model.

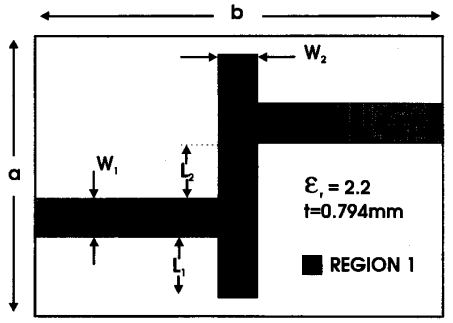

Fig. 3. Lowpass filter layout.

In order to illustrate the use of the region basis functions and the efficiency of the proposed set of functions a refined grid is used in the following model ($l_x = w_1/6 = 0.4064$ mm, $l_y = w_2/6 = 0.4233$ mm, $l_1 = 5.6896$ mm and $l_2 = 6.5024$ mm). This allows a closer approximation of the dimensions of the measured filter [2], without a large overhead in the number of basis functions required.

The circuit is divided into the five regions highlighted in Fig. 3. The criterion for sub-division into regions is such that a region is defined between each discontinuity. Two corners are present in region 1 (Fig. 3). The line mode basis functions Fig. 4 assume a simple straight line model (i.e. no corners). It is proposed that only two extra region basis functions are required to describe the perturbation of the current distribution from a simple straight line to region 1. Such a region basis function is illustrated in Fig. 2(e), note the inclusion of the corner singularity. The other regions are modelled by similar sets of precomputed basis functions which include a function for each corner in a region.

Results using this model are compared to measured $S$-parameters [2]. A fully shielded structure is assumed in this implementation therefore comparison to the open measured data [2] is affected by the proximity of the shield walls. For example, Figs. 6 and 7 show results for the identical models of the filter except the latter is housed in a box twice the length of the former. Comparison clearly indicates convergence to measured open response, for the larger box. Note, this is

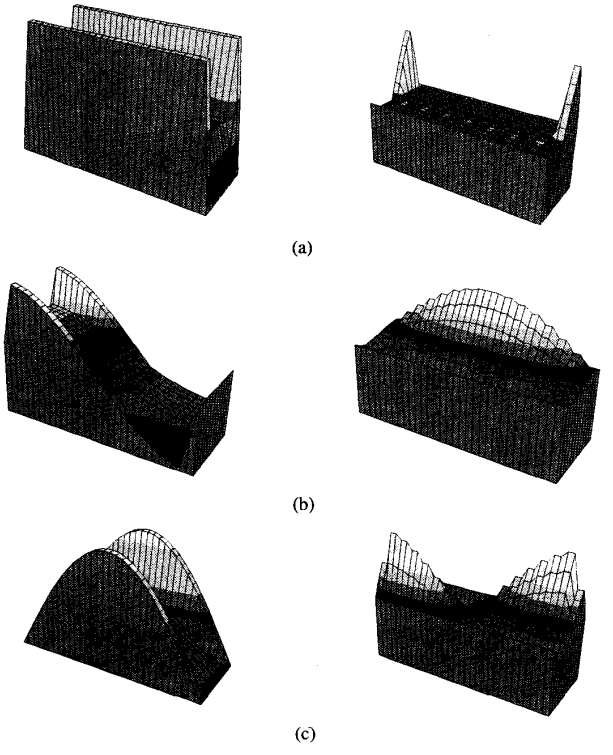


Fig. 4. Set of precomputed line mode basis functions: $X$ and $Y$ components.

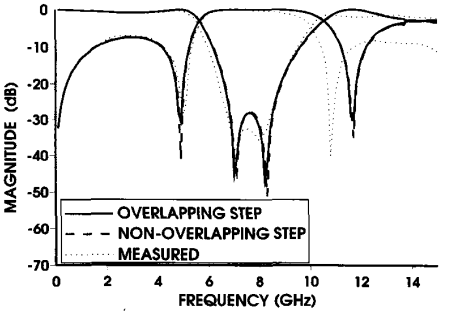


Fig. 5. Plot of $S$—parameters magnitude for simple lowpass filter; comparing overlapping and nonoverlapping step rooftop basis functions: Box 27.093mm × 10.16mm × 12mm.

limited by the introduction of box modes into the frequency band of interest.

Both models only required $P = 44$ (5) basis functions in total. An equivalent basic rooftop model requires $P = 305$ (for $b = 6.773$ mm in Fig. 8) rooftop basis functions. This results in a large decrease in CPU time as this is approximately proportional to $N^3$. The run-time on a HP9000series720 workstation, using nonoptimised code, was 3 seconds to calculate $S$-parameters at each spot frequency. The corresponding time for a basic rooftop algorithm was 400 seconds per spot frequency. Moreover a fine grid of rooftops could be defined with a resulting improvement in modelling the current singularities without an increase in the number of region basis functions required.

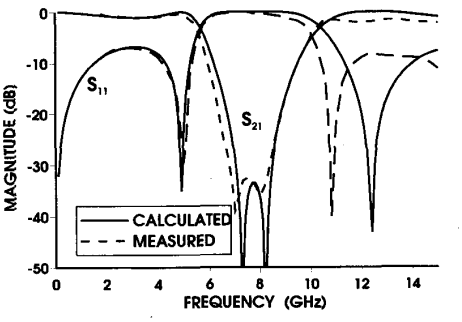


Fig. 6. Plot of $S$—parameters magnitude for simple lowpass filter model: Box 26.096mm × 6.7733mm × 8mm.

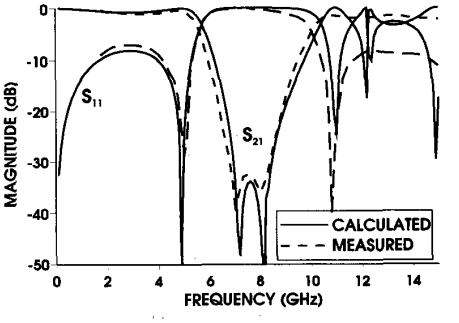


Fig. 7. Plot of $S$—parameters magnitude for simple lowpass filter model: Box 26.096mm × 13.5466mm × 8mm.

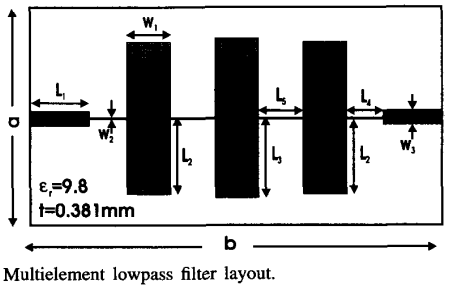


Fig. 8. Multielement lowpass filter layout.

## VI. Multi-Element Lowpass Filters

To illustrate the efficiency and accuracy of the region basis functions the analysis of the multi-element lowpass filter in Fig. 8 is outlined.

The technique assumes a fully shielded structure; shielded measured $S$-parameters are available for the lowpass filters of the form shown in Fig. 8. The structures are such that use of the basic rooftop technique is limited by the size of the matrix created by the large number of rooftops required. With reference to Fig. 8 and Table I the relative dimensions of the feedlines to the input lines and stubs results in a fine grid on the latter. A possible solution is to use different size rooftops for the feedlines and the stubs/input; but it is proposed that a more efficient use of region basis functions allows the full definition of the fine grid to be utilised, resulting in improved modeling of current singularities; with fewer functions than the former.

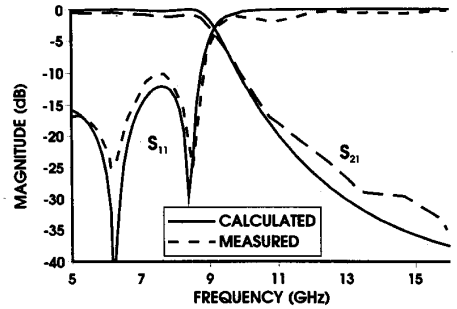


Fig. 9. Plot of $S$–parameters magnitude for multielement lowpass filter 1: Box $a = 6.4$mm, $b = 12.8$mm, and $h = 6$mm.

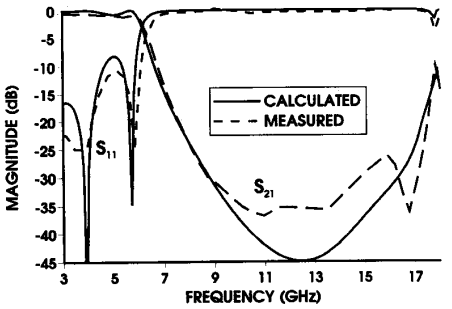


Fig. 10. Plot of $S$—parameters magnitude for multielement lowpass filter 2: Box $a = 3.2$mm, $b = 25.6$mm, and $h = 6$mm.

A set of region basis functions is used to model two different versions of the lowpass filter in Fig. 8, the dimensions of which are quoted in Table I. The input line is $14l_x$ wide (where $l_x = w_2/2 = 0.025$ mm) and $13l_y$ ($32l_y$ filter 2) long (where $l_y = 0.2$ mm), which for a basic rooftop model would result in 156 (403 filter 2) basis functions ($P$ in (5)) to just model the input line. A set of region basis functions can replace this with line modes and a single discontinuity function to compensate for the step in width, resulting in only 8 basis functions. The narrow microstrip lines are simply modeled with just a set of line modes. The stubs are modeled by a set of region basis functions similar to those described in [4] which include the end effect plus two functions to model the corners. In total only $P = 77$ (5) basis functions are needed resulting in a run-time on a HP9000series720 of 12 seconds per spot frequency to calculate $S$-parameters.

The $S$-parameters for the two filters are compared to the measured response in Figs. 9 and 10 respectively. A close match to the measured data is evident. $S11$ for the filters is modeled accurately both in the passband as well as the stop band. The difference between $S21$ predicted and measured in the passband is due to the lossless nature of the present model. An anomaly in the measured response is evident in $S21$ at approximately 12 GHz to 16 GHz for the second filter, Fig. 10, which is believed to be an inaccuracy in the measurements (note: $S21$ approx. $-30$ dB). This assumption is justified by the model accurately predicting the prominent feature at 18 GHz. Further comparison with an FDTD [3] model is currently being undertaken.

## VII. Conclusion

A general implementation of the SDM has been presented which efficiently characterizes planar microstrip circuits of arbitrary metallisation pattern. We have shown that sets of precomputed current basis functions can be defined which include *a priori* knowledge of the edge and corner singularities and allow the number of unknowns required to achieve a specified accuracy to be greatly reduced. This has led to the computer time being reduced by a factor of approximately 100. A library of such functions allows the rapid rigorous analysis of realistically complex circuits containing edges and corners. The ability to perform fast rigorous analyses will allow the effective use of optimisation routines for circuit design.

TABLE I
Dimension of Lowpass Filters

| filter | Dimensions (mm) | | | | | | | |
|---|---|---|---|---|---|---|---|---|
| | L1 | L2 | L3 | L4 | L5 | W1 | W2 | W3 |
| 1 | 2.6 | 1.0 | 1.2 | 1.o | 1.6 | 0.8 | 0.05 | 0.35 |
| 2 | 6.4 | 1.3 | 1.3 | 2.0 | 3.2 | 0.8 | 0.05 | 0.35 |

## Appendix A

### A. Asymptotic Greens Function and Impedance Matrix

The terms of Asymptotic Greens Function are defined as

$$hxx1 = hxy1 = -hyy1 = k_o/(2Z_o)$$
$$hxx2 = -hyy2 = 1/(1+\epsilon)$$
$$hxy2 = 0$$
$$K^{\infty}_{xx1} = \frac{\beta^2}{(\alpha^2+\beta^2)^{3/2}} \qquad K^{\infty}_{xx2} = \frac{\alpha^2}{(\alpha^2+\beta^2)^{1/2}}$$
$$K^{\infty}_{xy1} = \frac{\alpha\beta}{(\alpha^2+\beta^2)^{1/2}}$$
$$K^{\infty}_{yy1} = \frac{\alpha^2}{(\alpha^2+\beta^2)^{3/2}} \qquad K^{\infty}_{yy2} = \frac{\beta^2}{(\alpha^2+\beta^2)^{1/2}}$$

where $\alpha = n\pi/a$ and $\beta = m\pi/b$.

The partial asymptotic impedance matrix terms are defined as

$$Z^{\infty}_{\mathrm{st}1} = \sum_{n,m} \tilde{w}_t(n,m) K_{\mathrm{st}1}(n,m)^{\infty} \tilde{J}_s(n,m)$$
$$Z^{\infty}_{\mathrm{st}2} = \sum_{n,m} \tilde{w}_t(n,m) K_{\mathrm{st}2}(n,m)^{\infty} \tilde{J}_s(n,m)$$

and calculated by FFT.

## Appendix B

### A. Symmetry in Asymptotic Impedance Matrix

As detailed in [4], the algorithm calculates the DFT of a function $\mathbf{F}$ with the FFT algorithm and the elements of $Z^{\infty}_{\mathrm{st}}$ are evaluated using [4, (8)]. For the case of $Z^{\infty}_{xy}$ a sine[1] Fourier transform is used. Due to the Galerkin's formulation the testing and surface current functions are identical therefore during the

[1] Note: misprint in [4, Appendix].

evaluation of the elements of $Z_{xy}^{\infty}$ only half the matrix ($i \geq j$) need be calculated

$$\begin{aligned} Z_{xy}^{\infty}(i,j) = {} & 0.25\mathbf{F}\left(\frac{x_i - x_j}{a}, \frac{y_i - y_j}{b}\right) \\ & + S * 0.25\mathbf{F}\left(\frac{x_i + x_j}{a}, \frac{y_i - y_j}{b}\right) \\ & - S * 0.25\mathbf{F}\left(\frac{x_i - x_j}{a}, \frac{y_i + y_j}{b}\right) \\ & - 0.25\mathbf{F}\left(\frac{x_i + x_j}{a}, \frac{y_i + y_j}{b}\right) \end{aligned} \tag{10}$$

where $S$ is a sign function

$$S = \begin{cases} 1 & \text{if } i \geq j \\ -1 & \text{otherwise} \end{cases}$$

and $i$ and $j$ correspond to the $i^{\text{th}}$ and $j^{\text{th}}$ basis and testing functions respectively. The implementation of the FFT algorithm symmetry is critical for the case of sets of region basis functions defined on a fine grid. That is, when each basis function is comprised of the order of 100's of component sub-domain rooftop functions.

## ACKNOWLEDGMENT

The authors wish to thank Prof. J. P. McGeehan for provision of facilities at the Centre for Communications Research, SERC UK and Elettronica (U.K.) Ltd. for financial support and are grateful to Elettronica (U.K.) Ltd. for supplying the measured response of the multi-element filters.

## REFERENCES

[1] R. W. Jackson, "Full-wave, finite element analysis of irregular microstrip discontinuities," *IEEE Trans. Microwave Theory Tech.*, vol. 37, pp. 81–89, Jan. 1989.

[2] D. M. Sheen, S. M. Ali, M. D. Abouzahra, and J. A. Kong, "Application of the three-dimensional finite-difference time-domain method to the analysis of planar microstrip circuits," *IEEE Trans. Microwave Theory Tech.*, vol. 38, pp. 849–857, July 1990.

[3] D. Paul, E. M. Daniel, and C. J. Railton, "Fast finite difference time-domain method for the analysis of a planar microstrip filter," *21st European Microwave Conf. Proc.*, Stuttgart, Germany, 1991, pp. 303–308.

[4] C. J. Railton and S. A. Meade, "Fast rigorous analysis of shielded planar filters," *IEEE Trans. Microwave Theory Tech.*, vol. 40, pp. 978–985, May 1992.

[5] W. Wertgen and R. H. Jansen, "Novel Green's function database technique for the efficient full-wave solution of complex irregular ($M$) MIC-structures," *19th European Microwave Conf. Proc.*, London, England, 1991, pp. 199–294.

[6] C. J. Railton and J. P. McGeehan, "A rigorous and computationally efficient analysis of microstrip for use as an electro-optic modulator," *IEEE Trans. Microwave Theory Tech.*, vol. 37, pp. 1099–1104, July 1989.

[7] J. C. Rautio and R. F. Harrington, "An elecromagnetic time-harmonic analysis of shielded microstrop circuits," *IEEE Trans. Microwave Theory Tech.*, vol. MTT–35, pp. 726–730, Aug. 1987.

[8] T. Becks and I. Wolff, "Analysis of 3-D metallization structures by a full-wave spectral domain technique," *IEEE Tans. Microwave Theory Tech.*, vol. 40, pp. 2219–2227, Dec. 1992.

**S. A. Meade** was born in Taunton, Somerset, England, in 1968. He received the B.Eng. degree in electrical and electronic engineering from the University of Bristol in 1990. He is currently pursuing the Ph.D. at the same university.

His research interests include the application of the Spectral Domain method to modeling complex planar circuits and the finite-difference time-domain method to the analysis of antennas.

**Chris J. Railton** (M'88), for a photograph and biography see page 1212 of the July issue of this TRANSACTIONS.